Optimizing Interfacial Cross-Linking in Graphene-Derived Materials, Which Balances Intralayer and Interlayer Load Transfer

Enlai Gao,[†][iD] Yu Cao,[‡] Yilun Liu,*[,§] and Zhiping Xu*[,†,⊥][iD]

[†]Applied Mechanics Laboratory, Department of Engineering Mechanics and Center for Nano and Micro Mechanics, Tsinghua University, Beijing 100084, China

[‡]College of Chemistry, Nankai University, Tianjin 300071, China

[§]State Key Laboratory for Strength and Vibration of Mechanical Structures, School of Aerospace Engineering, Xi'an Jiaotong University, Xi'an 710049, China

[⊥]Applied Mechanics and Structure Safety Key Laboratory of Sichuan Province, School of Mechanics and Engineering, Southwest Jiaotong University, Chengdu, Sichuan 610031, China

S *Supporting Information*

ABSTRACT: Graphene-derived layer-by-layer (LbL) assemblies in the form of films or fibers have recently attracted particular interests owing to their low cost, facile fabrication, and outstanding mechanical properties, which could be further tuned by surface functionalization that cross-links graphene sheets in the assembly. However, this interfacial engineering approach has not yet been finely utilized considering the dual roles of cross-links in modifying the intrinsic properties of graphene sheets and their interlayer interactions. In this work, combining first-principles calculations and continuum-mechanics-based model analysis, we find that the functionalization weakens the intrinsic mechanical resistance of graphene, whereas it enhances interlayer load transfer through interlayer cross-linking. There are optimum cross-linking densities or concentrations of the surface functional groups that maximize the overall tensile stiffness, tensile strength and strain to failure of graphene-derived LbL assemblies, arising from the competition between intralayer and interlayer load-bearing mechanisms, as defined by the type of functionalization and size of graphene sheets. Our work quantifies the ultimate mechanical performance of graphene-derived LbL assemblies, on the condition that their microstructures and functionalization could be adequately controlled in the fabrication process.

KEYWORDS: *graphene-derived materials, layer-by-layer assembly, interlayer cross-links, first-principles calculations, load transfer, optimum design*
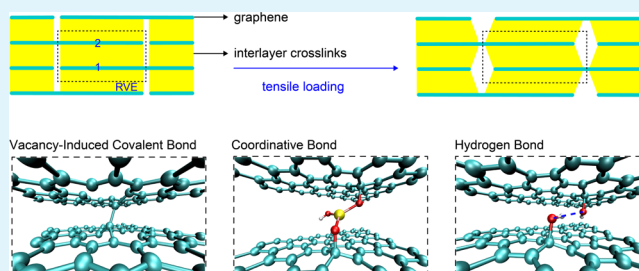
INTRODUCTION

Graphene has attracted particular interests due to its high intrinsic tensile stiffness and strength up to 1 TPa and 120 GPa and a strain to failure of 20%. Recently, much attention has been paid on how to bring the strong and tough merits of graphene monolayers into those of their macroscopic forms.[1−5] Within this scenario, one could employ graphene nanostructures as reinforcing phases in composites.[6,7] However, the native interfaces between graphitic nanostructures and matrices create weak points where failure may initiate. This issue critically prevents successful transfer of the outstanding performance of graphene across multiple length scales up to the macroscopic level. In addition, the lack of an efficient technique to uniformly disperse graphene-based nanostructures into the matrix further limits the overall reinforcement.[7,8] An alternative approach to macroscopic mechanical applications of graphene and its derivatives (e.g., graphene oxides) is to assemble them in a layer-by-layer (LbL) manner, with high microstructural orders (Figure 1a).[6,9−13] Studies have shown

that the interlayer cross-linking mechanism and the size of the graphene sheet are two of the most important factors in determining the overall mechanical performance of graphene-derived films and fibers. For example, the tensile strength (strain at failure) of graphene films ranges from 189 MPa (2.7%) to 425 MPa (2.6%) with different types of interlayer cross-links,[14,15] and the tensile strength (strain at failure) of graphene fibers is 140.0 MPa (5.8%) and 501 MPa (6.7%) for the lateral size of the graphene sheet of 0.84 and 18.5 μm, respectively.[16,17] Indeed, similar layered hierarchical microstructures appear in many biological materials, including bones, teeth, and nacre, where brittle minerals and soft proteins are integrated in a staggered order for superior stiffness, strength, and toughness,[18−26] which can be captured in the tension-shear chain model that includes the intralayer and interlayer load
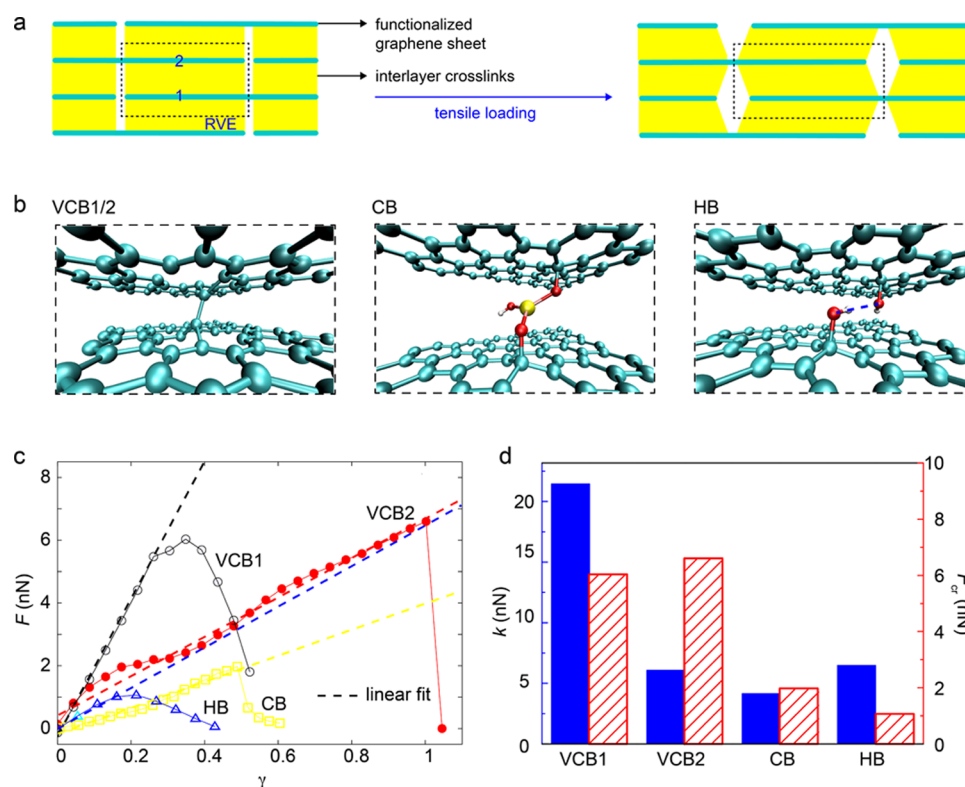
Figure 1. (a) Deformable tensile-shear (DTS) model before and after tensile loading is applied. The representative volume element (RVE) containing two sheets (1 and 2) is denoted by the dashed box. (b) Detailed atomic structures of the cross-links considered in this work, which include the vacancy-induced covalent bond (VCB1&2), the divalent atom (magnesium)-assisted coordinative bonds (CBs), and the hydrogen bond formed between two hydroxyl groups (HB). (c) Shear force−strain relation, (d) shear stiffness, and force to failure calculated for a graphene bilayer bridged by VCB, CB, and HB cross-links.

transfer mechanisms.[19,20,27] Inspired by the similar LbL microstructures, a deformable tension-shear (DTS) chain model considering the intralayer deformation was proposed[1,2] to predict the overall mechanical properties of graphene-derived LbL materials. Recent studies further explored topologically optimized staggered LbL structures for high mechanical performance.[4,5,19,26,28] However, compared to the above-mentioned LbL biological materials with microscale building blocks, interlayer cross-linking between single-atom-thick graphene sheets remarkably reduces their in-plane mechanical resistance. Consequently, enhancing the interlayer load transfer by cross-linking will not always improve the overall mechanical properties of the LbL assemblies. More interestingly, the graphene-based films or fibers are reminiscent of carbon fibers consisting of graphitic building blocks, although their microstructures have not been well elucidated at present. However, the state-of-the-art performance of graphene-derived films or fibers is still less competitive than that of carbon fibers, which may be attributed to the high density of defects and larger interlayer distances between graphene sheets in these LbL assemblies. Considering the complexity in their hierarchical structures and cross-linking mechanisms, there is still a lack of rigorous understanding of the fabrication−microstructure−properties relationship, which prevents us from being able to rationally design graphene-derived materials with superior mechanical performance.

Load transfer through native interfaces with van der Waals interaction between graphene sheets is weak, commonly leading to pull-out failure of the reinforced phases from the matrix.[8,29,30] Technological advances in modifying gra-

phene[2,11,12,31−35] by functional groups and the implementation of various cross-linking mechanisms, including multimodality, sacrificial, and self-healing bonds,[33,36−38] have enabled optimum design of the LbL assemblies by engineering material interfaces at the molecular level. Recently, the effects of interlayer cross-links in this context have been reported in several experimental[31,32] and computer simulation-based studies,[39,40] wherein graphene sheets are cross-linked by covalent, coordinative, or hydrogen bonds introduced through processes of oxidation,[41] reduction,[42] and irradiation treatments.[43] These approaches substantially improve the interfacial load transfer capacity and thus elevate the overall mechanical properties, even though chemical treatments can introduce defects such as vacancies and adatoms in graphene and reduce its in-plane mechanical resistance as an accompanying effect.[29,30,44] As an evidence, experimental studies demonstrated mechanical degradation of the LbL assemblies after excess radiation, although the cross-links lead to enhancement at a low concentration.[29,44]

In this work, we aim to propose stiffening, strengthening, and toughening strategies for graphene-derived LbL materials by optimizing the concentration of various functional groups on the basis of first-principles calculations and continuum model analysis. The competition between the weakening intralayer mechanical resistance and enhancement in the interlayer load transfer after the interfacial engineering is discussed. Three representative types of surface functionalization and interlayer cross-linking mechanisms that have been reported in experimental work are considered, including the VCBs,[43] CBs,[2,33] and hydrogen bonds (HBs).[39,45] Their atomic

structures are illustrated in Figure 1b. For VCB, two carbon atoms in the neighboring graphene sheets are covalently bonded across the layers, leaving a monovacancy in each layer after the cross-link forms. This covalent cross-link is reminiscent of the "extended interplanar linking" in graphite.[43] For CB, a divalent metal atom (Mg in this study) in the interstitial space bridges the hydroxyl groups on the graphene sheets, following previous work.[33] For HB, two hydroxyl groups bonded to the top and bottom graphene layers interact through the hydrogen bonds.[39] In the following part, computational methods and theoretical models will be described first, followed by results and discussion. Phase diagrams of the overall mechanical properties predicted for graphene-derived LbL materials in the spaces of designing parameters (the concentration of functional groups, the size of graphene sheet size) are predicted, and the optimum cross-linking densities (OCDs) are obtained for the highest tensile stiffness, strength, and strain to failure, respectively.

■ MATERIALS AND METHODS

First-Principles Calculations. We explore the structural and mechanical properties of graphene sheets and their interfaces with various functional groups by performing first-principles calculations using the plane-wave basis set-based density functional theory (DFT) methods. The Perdew−Burke−Ernzerhof parameterization[46] of generalized gradient approximation (GGA) is used for the exchange-correlation functional, and the DFT-D3 method with Becke−Johnson damping is used for the corrections of the interlayer van der Waals interaction (Figure S1).[47,48] The projector augmented wave potentials[49] are used for ion−electron interactions. The Vienna ab initio simulation package (VASP) is employed for all calculations.[50] For all results presented, an energy cutoff of 400 eV is used for the plane-wave basis sets. A single Γ-point is used for the Brillouin zone integration as we have relatively large supercells. These settings have been verified to achieve a total energy convergence of less than 1 meV/atom. For geometry relaxation, the force on atoms is converged below 0.01 eV/Å. All structures are initially optimized using the conjugated gradient method. A vacuum layer of 20 Å is used to isolate the atomic layer.

Characterization of Mechanical Properties. The key parameters to be determined are the in-plane mechanical properties of the graphene sheet with various functional groups and the interlayer shear mechanical properties of the interlayer cross-link generated by different types of functional groups. In-plane tensile behaviors of a graphene sheet with various functional groups are investigated by directly applying an in-plane tensile deformation in the armchair and zigzag directions of a rectangular supercell of the monolayer graphene with a lateral size of 1.97 nm × 1.71 nm, with 0, 1, 2, and 4 randomly distributed functionalized groups. The composite performance of the cross-linked bilayer graphene is also calculated to assess the effect of the interlayer interaction, which is the same as the functionalized monolayer (Figure S2a), indicating that the in-plane deformation and failure mechanisms are independent of the interlayer interaction as its shear is not involved. The supercell size effect is assessed, and the current setup is large enough compared to that of the structural distortion induced by functionalization (Figure S2b). Geometrical optimization is performed at each step with a predescribed strain on the supercell, corresponding to a quasi-static strain loading condition. The stress−strain relationship under tensile loading along the armchair and zigzag directions demonstrates similar values of tensile stiffness and strength. In our following discussion, their averaged value will be used. The mechanical properties of the interlayer cross-links between adjacent graphene sheets are studied by applying shear deformation to a rhombic supercell of 1.72 nm × 1.72 nm consisting of two parallel graphene sheets and one interlayer cross-link. The shear deformation is applied by transversely moving one graphene sheet with respect to its neighbor, step by step. The shear force−displacement relationship

in the armchair and zigzag directions show similar shear strength as reported in our previous work,[2,33] and we will use the value for shear along the armchair direction in the following discussions unless otherwise noted. After the rigid displacement between the two sheets, or in other words, after the interlayer shear is applied, the degrees of freedom of all carbon atoms in the shear direction are fixed, whereas those in the other two directions are freely relaxed in a geometrical optimization step. The interlayer shear force is calculated by summing up all forces acting on the carbon atoms of one graphene layer in the shear direction. It should be noted that the equilibrium structures are obtained by a combined optimization of local structures of the functional groups and the lattice distortion induced in graphene in the supercell, which is a natural description of the dependence of the interlayer shear resistance on the cross-linking density.

DTS Model and Failure Mode Selection. Considering the LbL hierarchy of graphene-derived materials and the finite size of the graphene sheet in them, the in-plane tensile load in the graphene sheet has to be transferred to its neighboring sheets by deforming the interlayer cross-links. The DTS model that considers the interlayer cross-links as a continuum medium under shear is used here to predict the overall mechanical behaviors, as illustrated in Figure 1a. The unidirectional tensile load applied at the ends of the samples is transferred along a path consisting of both the sheets under tension and the interlayer cross-links under shear. On the basis of the RVE in Figure 1a, we consider a tensile force, F_0, applied on the RVE. According to the DTS model, an effective tensile stiffness or Young's modulus Y_{eff} for the whole structure is defined as $(F_0/2h_0)/(\Delta/l)$, where $F_0/2h_0$ is the effective tensile stress and $\Delta = [u_1(l) - u_2(0)]$ is the elongation of the RVE cell, which can be explicitly expressed as

$$Y_{eff} = \frac{D}{2h_0\{0.5 + [(1 + c)/s](l_0/l)\}} \quad (1)$$

Here, u_1 and u_2 are the displacement fields in neighboring sheets 1 and 2 as a function of position x measured from the left side of RVE ($x = 0$), that is, the free end of the lower sheet 1 in Figure 1a. According to the staggered arrangement of sheets in the RVE, the free end of one sheet has the same coordinate x as the center of its neighboring sheets. h_0 is the interlayer distance, $s = \sinh(l/l_0)$, $c = \cosh(l/l_0)$, and l is the size of RVE or the half-sheet length. We define here a parameter $l_0 = (Dh_0/4G)^{1/2}$ to characterize the length scale of effective interlayer load transfer through parameters obtained from our first-principles calculations, including the interlayer distance, h_0, the effective shear modulus of the interlayer cross-links, G, and tensile stiffness of the functionalized graphene sheet, $D = Yh$, where Y and h are its tensile modulus and thickness, respectively.

In addition to the effective tensile stiffness, Y_{eff}, the tensile strength and strain to failure are the other two important mechanical parameters. Under tensile loading, graphene-derived materials could fail in two distinct modes, that is, the fracture of the functionalized graphene sheet when the tensile stress in the graphene sheet is above a critical value, $\sigma > \sigma_{cr}$ (denoted as mode G), or failure of interlayer cross-links when the interlayer shear strain exceeds a critical value, $\gamma > \gamma_{cr}$ (mode I). Therefore, the tensile strength of graphene-derived LbL materials is the lower value selected from these two failure modes, that is

$$\sigma_s = \min\begin{cases} \dfrac{\sigma_{cr}h}{2h_0} & \text{(mode G)} \\[2ex] \dfrac{Ds\gamma_{cr}}{2(1+c)l_0} & \text{(mode I)} \end{cases} \quad (2)$$

Similarly, the strain to failure of the material is the minimum value of those in modes G and I

$$\varepsilon_s = \min \begin{cases} \dfrac{\sigma_{cr}h}{2D} + \dfrac{\sigma_{cr}h}{D}\dfrac{l_0}{l}\dfrac{1+c}{s} & \text{(mode G)} \\[2ex] \dfrac{\gamma_{cr}h_0}{2l_0}\dfrac{s}{1+c} + \dfrac{\gamma_{cr}h_0}{l} & \text{(mode I)} \end{cases} \tag{3}$$

Here, the first and second terms (in both modes G and I) are the contributions from the intralayer elongation and interlayer shear, respectively. The criterion of the selection of the failure modes is determined by both structural and mechanical properties of the functionalized graphene sheet and interlayer cross-links, that is

$$\begin{cases} \dfrac{\sigma_{cr}h}{D\gamma_{cr}} \leq \dfrac{h_0 s}{l_0(1+c)} & \text{(mode G)} \\[2ex] \dfrac{\sigma_{cr}h}{D\gamma_{cr}} \geq \dfrac{h_0 s}{l_0(1+c)} & \text{(mode I)} \end{cases} \tag{4}$$

Detailed derivation for eqs 1–4 can be found in our previous report.[1,2]

■ RESULTS AND DISCUSSION

Mechanical Properties of Interlayer Cross-Links under Shear. To characterize the mechanical properties of an interlayer cross-link between graphene sheets (Figure 1a,b), we can define the interlayer shear stiffness as k and shear strength as F_{cr}, on the basis of a linear elastic approximation

$$F = k\gamma(F < F_{cr}, \gamma < \gamma_{cr}) \tag{5}$$

where F and γ are the shear force and strain of the cross-linking continuum in the DTS representation, where the cross-links are stretched as the cross-linked graphene sheets are displaced with respect to each other. F_{cr} and γ_{cr} are the interfacial shear strength and strain to failure following this definition. The values of $F(F_{cr})$, $\gamma(\gamma_{cr})$, and k obtained from our first-principles calculations are summarized in Figures 1c,d (F_{cr} and γ_{cr} are determined from the point of curves where shear force starts to decline). For VCB, the direct covalent bonding between neighboring graphene sheets leads to a much higher interfacial shear strength (~6 nN) than those for CB or HB. The interlayer distance with VCBs is almost the same as that for graphite, that is, $h_0 = 0.342$ nm. The configuration of the VCB cross-link is asymmetric along the armchair direction (Figure S3) and thus the VCB-cross-linked interface along the positive and negative directions presents different shear stiffness and strain to failure but similar shear force to failure. We name the cross-linking mechanism with the top-layer graphene displaced from the left to the right as VCB1 and that with the opposite shear direction as VCB2 (Figure 1b). The critical shear strain calculated for VCB1 and VCB2 is 0.348 and 1.002, respectively. For the CB-based cross-link, the ligands (hydroxyl groups and oxygen atoms bonded to graphene) offer electron pairs to form a complex with metal atoms or ions, which are able to reform after dissociation under mechanical perturbation because of its lower directional dependence.[33,51] Our first-principles calculations show that the Mg-based coordinative complex leads to an interfacial shear force to failure, $F_{cr} = 1.98$ nN, which is defined as the force amplitude where the bond between Mg and oxygen atoms attached to the graphene sheet breaks, and the interlayer distance for CB is 0.695 nm. For HB, the interfacial shear force to failure is 1.07 nN and the interlayer distance is 0.374 nm. These mechanical properties obtained from our first-principles calculations for the three types of cross-links are summarized in Table 1.

Table 1. Intralayer and Interlayer Structural/Mechanical Parameters As Introduced in Equations 5, 6a, 6b, 7a and 7b, Which Are Calculated for Graphene-Derived LbL Materials Cross-Linked through VCB1&2, CB, and HB, Respectively

	α	β	k (nN)	F_{cr} (nN)	γ_{cr}	d (nm)
VCB1	9.44	75.8	21.46	6.04	0.348	0.342
VCB2	9.44	75.8	6.09	6.61	1.002	0.342
CB	2.48	29.3	4.15	1.98	0.489	0.695
HB	2.61	7.00	6.48	1.07	0.214	0.374

It should be remarked here that in the discussion above, we study only one cross-link in the supercell that is large enough to exclude mutual interaction between the cross-link under consideration and its periodic images. Consequently, these mechanical parameters can be applied to isolated cross-links and can be extended to distributed cross-links on the condition that the concentration is low, wherein the interaction or cooperation between different cross-links is weak enough to be neglected. The cooperative effects at graphene interfaces with high-density cross-links, although important and interesting, will be explored in our future studies. In this limit, interlayer load transfer is the multiplication of the individual cross-links, and the interlayer shear stiffness and force to failure are proportional to the concentration of functional groups or the interlayer cross-link density. With this assumption, we define the concentration of functional groups in a graphene sheet as ϕ, which is defined as N_I/N_C. Here, N_C is the number of carbon atoms in pristine graphene, whereas N_I is the number of functional groups. In the following analysis, we assume that each interlayer cross-link involves two functional groups in the neighboring graphene sheets, which is reasonable for the three types of cross-linking mechanisms we consider in this work. The effective interlayer shear modulus, G, and interfacial shear strength, τ_s, are thus

$$G = k\phi/f \tag{6a}$$

$$\tau_s = k\gamma_{cr}\phi/f \tag{6b}$$

where $f = 0.026$ nm^2 is the area of each carbon atom in graphene. In addition, from eq 3 we can also see that the value of γ_{cr} has a significant effect on the overall strain to failure of graphene-derived LbL materials.

Intralayer Mechanical Resistance of Functionalized Graphene. The key parameters for the mechanical resistance of the graphene sheet under tension in the DTS model include its tensile stiffness, strength, and strain to failure. As functionalized groups are introduced into the graphene sheets, the sp^2 covalent network is perturbed or even destroyed. Previous studies demonstrated that the tensile stiffness, D, and tensile strength, σ_{cr}, of the graphene sheet could be related to the concentration of the functional groups, ϕ, in the following forms[52–54]

$$D = D_0(1 - \alpha\phi) \tag{7a}$$

$$\sigma_{cr} = \sigma_c/(1 + \beta\phi)^{0.5} \tag{7b}$$

where D_0 and σ_c are the tensile stiffness and strength of pristine graphene, and the reduction factors α, β are functionalization-specific parameters that characterize the significance of ϕ-dependence. These parameters were obtained from our DFT calculations. The higher the values of α and β, the more
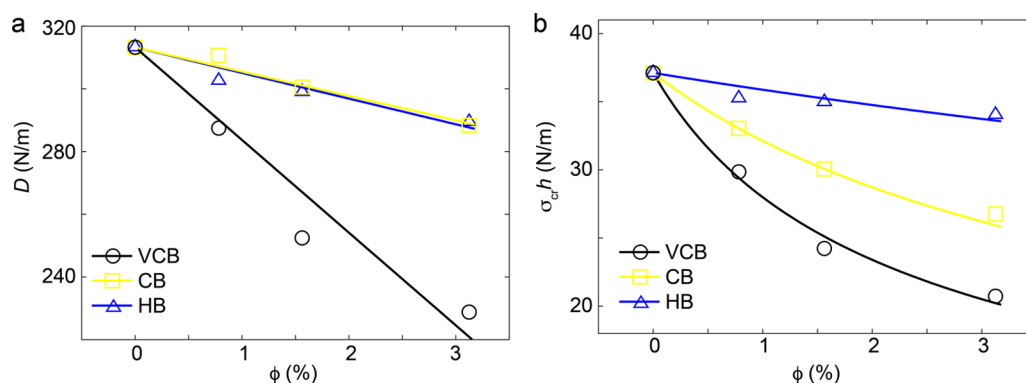
Figure 2. Dependence of in-plane (a) tensile stiffness and (b) tensile strength of a graphene sheet functionalized by the VCB, CB, and HB cross-links.
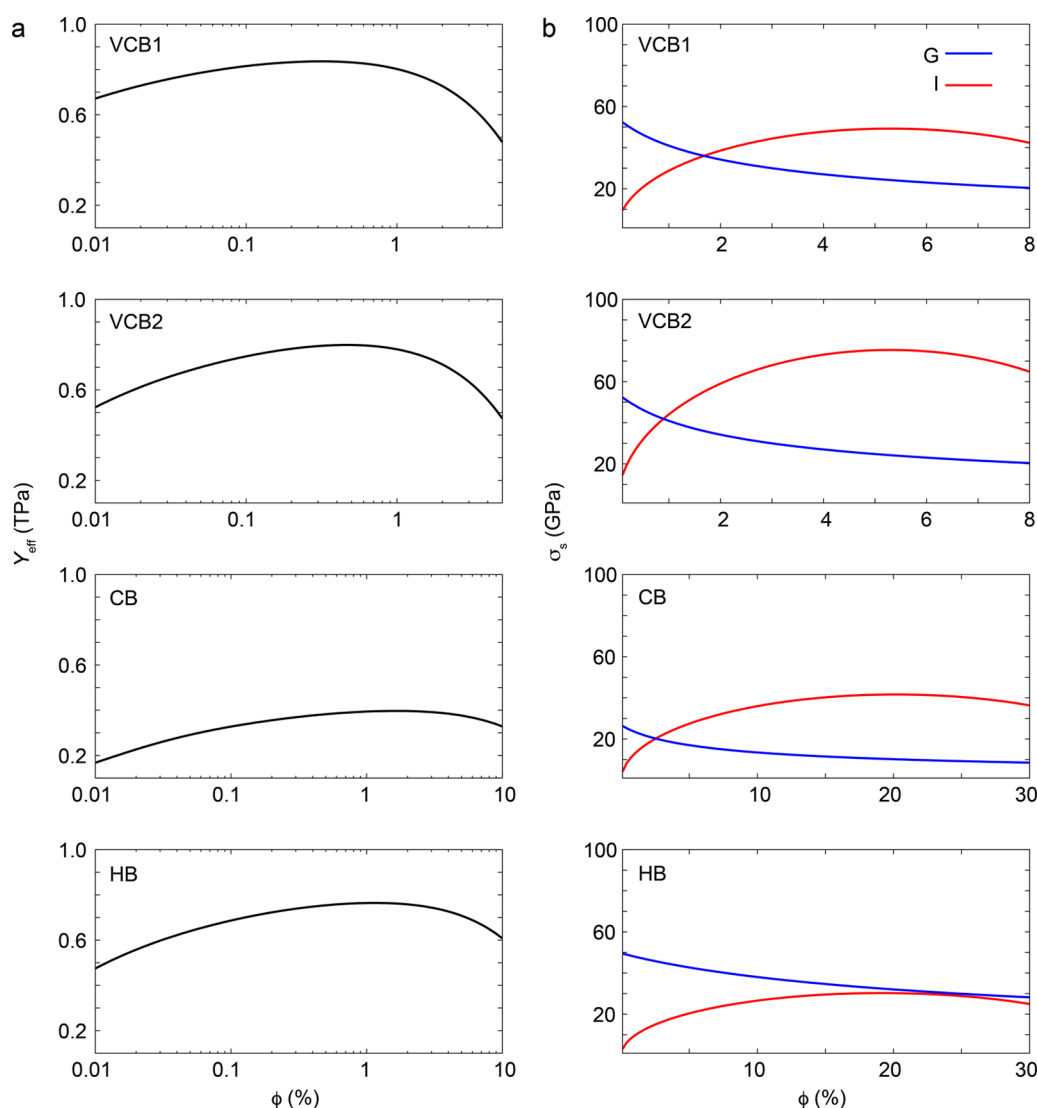

Figure 3. Dependence of the overall (a) tensile stiffness and (b) tensile strength of graphene-derived LbL materials on the concentration of VCB, CB, and HB cross-links for a typical graphene sheet with a lateral size of 100 nm. There are two failure modes (mode G for intralayer fracture, and mode I for interlayer failure). For mode G (the blue line in panel b), the tensile strength decreases monotonically with the concentration of cross-links, whereas for mode I, the tensile strength (the red line in panel a) increases first, reaches a peak value at the critical concentration, and then decreases.

significant reduction on the mechanical resistance of graphene sheets the defect could lead to.

On the basis of our first-principles calculations, we assume that the functional sites in graphene are randomly distributed and uncorrelated. Thus, eqs 7a and 7b can be applied to fit
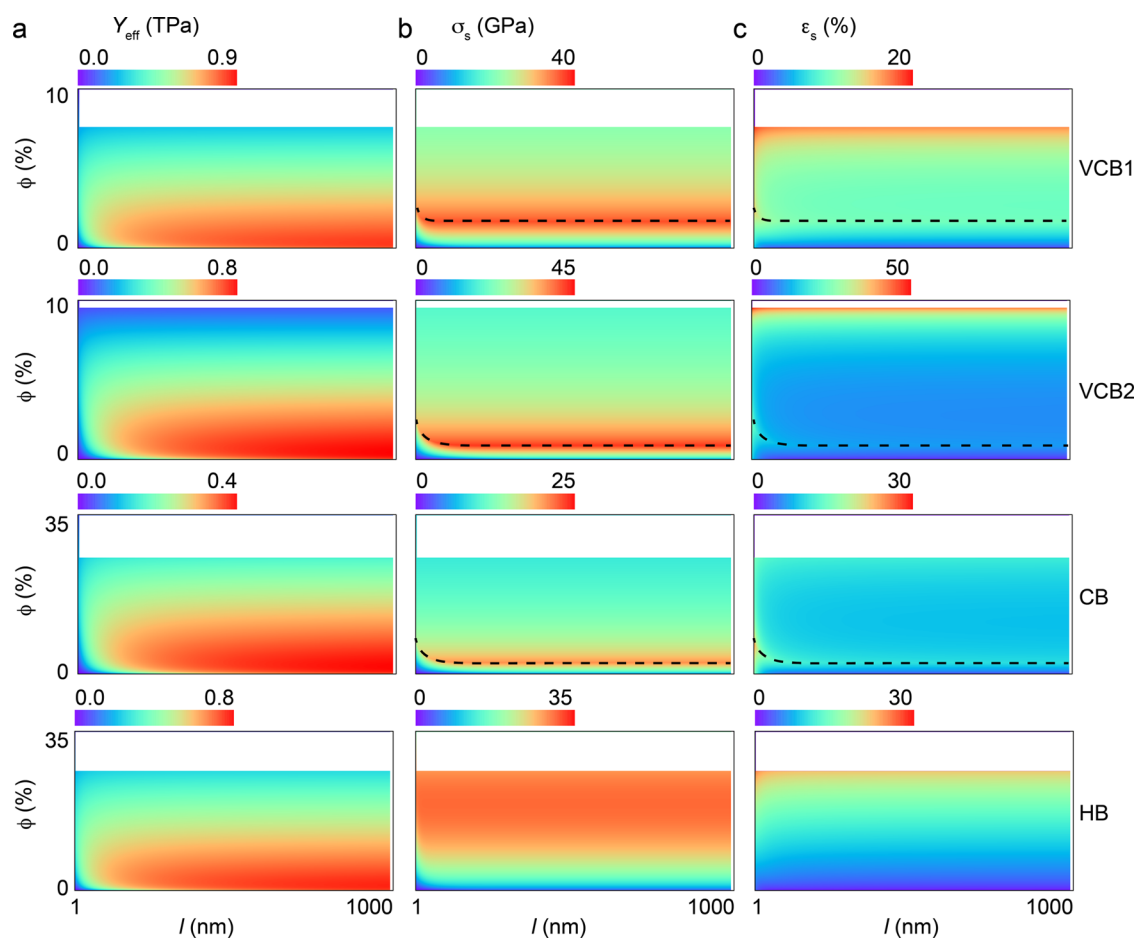
Figure 4. Values of (a) tensile stiffness, (b) tensile strength, and (c) strain to failure calculated as a function of the cross-linking density, the lateral size of the graphene sheets, and the type of cross-links (VCB1, VCB2, HB, and CB) for the graphene-derived LbL materials. The dashed line in the plots of tensile strength and strain to failure indicates the transition from interlayer failure (mode I, below the dashed line) and intralayer fracture (mode G, above the dashed line) failure (for HB, only mode I failure applies). The blank space is for graphene-derived LbL materials with $l_0 = (Dh_0/4G)^{1/2} < h_0$.
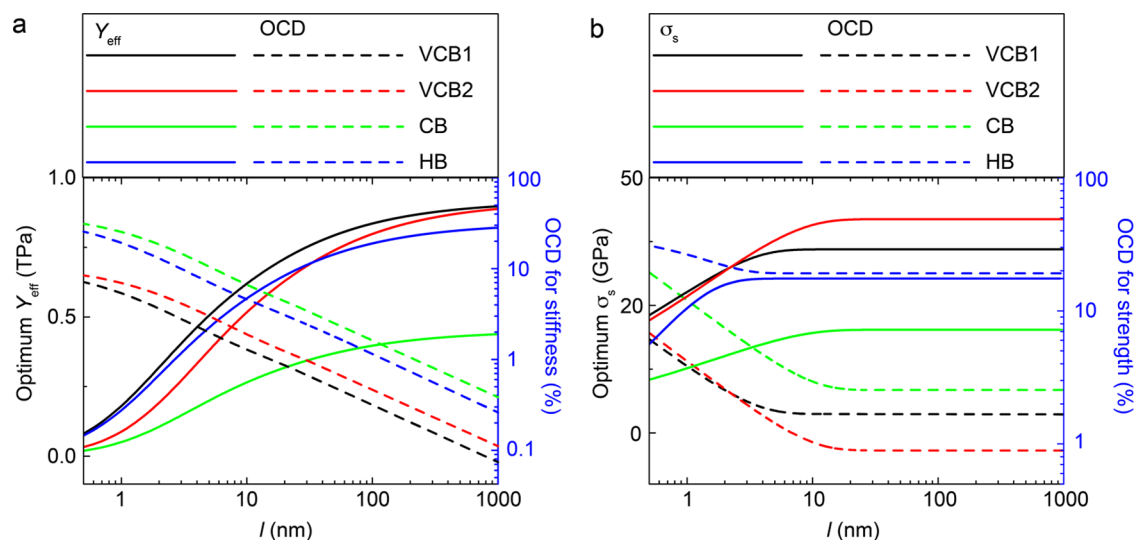

Figure 5. (a) Effective tensile stiffness Y_{eff} (solid lines) at the OCD (dashed lines) for tensile stiffness predicted graphene-derived LbL materials with four types of cross-linkers and sheet size l. (b) Same plots for the overall tensile strength, σ_s (solid lines), at the OCD (dashed lines) for tensile strength.

parameters α and β for the three representative functional groups (VCB, CB, HB). The results are shown in Figure 2 and

summarized in Table 1. From the calculation results, we find that the VCB reduces in the in-plane tensile stiffness and

strength most significantly. The CB and HB have similarly weaker effects on the stiffness of the graphene sheet as the lattice is less distorted, in a similar way for CB and HB at small strain levels. However, the reduction in the tensile strength at the same concentration is much more significant for CB than that for HB as the graphene lattice is more significantly perturbed by the CB functionalization. The reduction in Young's modulus and tensile strength of functionalized graphene induced by the functional groups can also be visualized through the charge depletion during loading processes (Figure S4), which shows that the functionalization perturbs covalent bonds in graphene locally and nucleates fracture of the structures, which lead to the reduction in tensile stiffness and strength.

Optimum Design of Graphene-Derived LbL Materials. The intralayer and interlayer mechanical properties quantified by our first-principles calculations clearly indicate that the introduction of functional groups and cross-links enhances the interlayer shear resistance but reduces the in-plane tensile resistance. Consequently, there should be an OCD to maximize the overall effective tensile stiffness, Y_{eff}, and tensile strength, σ_s, which can be determined by the DTS model.

From eq 1 and the values of D, G, and h_0 calculated for cross-links VCB1, VCB2, CB, and HB, we first calculate Y_{eff} for graphene-derived LbL materials with sheet size $l = 100$ nm for various cross-linking densities ϕ (Figure 3a). The results show that Y_{eff} first increases with ϕ and then decreases after a peak value. The OCD to maximize Y_{eff} can be calculated as

$$\partial Y_{eff}/\partial \phi = 0 \tag{8}$$

Furthermore, Y_{eff} is plotted as a function of the cross-linking density, the lateral size of graphene sheets, and the type of cross-links for graphene-derived LbL materials in Figure 4a. The l-dependence of OCD for the tensile stiffness and the value of Y_{eff} at the OCD are plotted in Figure 5a, which shows that the optimum value of Y_{eff} increases with l first and then becomes saturated for $l \gg l_0$ while the load transfer between neighboring layers becomes sufficient. The highest value of Y_{eff} is D_0/h_0, which can be achieved in the limit with $l \gg l_0$ and $\phi = 0$, as in the situation of graphite (Figure 4a). The ultimate values of the effective tensile stiffness for VCB1&2, HB, and CB cross-links are ~0.9, 0.4, and 0.8 TPa, respectively. Here in the definition of Y_{eff}, we use the interlayer distances of cross-linked interfaces as the thickness of the functionalized graphene sheets, which are obtained from first-principles calculations and considered to be uniform in the whole LbL material (Figure 5a). It should be remarked here that we neglected the variation of the interlayer distance in calculating the values of tensile stiffness and strength as the functional groups are nonuniformly distributed at the interlayer gallery, which could be introduced through an effective factor and should not affect our prediction of OCD significantly.

To determine the overall tensile strength of graphene-derived LbL materials, it is noted that it could fail in one of the two distinct modes (graphene intralayer fracture mode G or interlayer failure mode I). The one with the lower tensile strength is selected as the failure mode. With eqs 2, 5, 6b, and 7b and parameters γ_{cr} and h_0 obtained for VCB1, VCB2, CB, and HB, we conclude from Figure 3b for $l = 100$ nm that σ (the lower values in two data sets) also increases first with ϕ before reaching a peak value in mode I as the cross-links improve the interlayer load transfer. After reaching the peak, σ decreases with ϕ in mode G as the functional groups weaken the

graphene sheets. The transition in the failure modes depends on the values of l and ϕ (Figure 4b; for HB, only mode I failure applies). The OCD for the ultimate tensile strength, σ_s, and the value of σ_s at the OCD can be determined from eq 4, showing that the ultimate values of σ_s for VCB1, VCB2, HB, and CB are ~36, 42, 30, and 20 GPa, respectively (Figure 5b). It should be noted that the difference of the ultimate tensile strength value is also attributed to changes in the interlayer distance, in addition to the competition between reduction in the in-plane resistance and enhancement in the interlayer shear resistance. The maximum values of Y_{eff} and σ_s are attained at different ϕ values and thus a compromise has to be made between high stiffness and high strength in design.

Furthermore, the overall strain to failure also is a very important mechanical parameter for the material that quantifies its toughness. Our results show that as the cross-link density increases, the intralayer tensile stiffness, D, decreases, whereas the interlayer shear modulus increases and thus the strain to failure increases, according to eq 3. Considering the practical interest, we calculate the strain to failure of graphene-derived LbL assemblies of $l_0 = (Dh_0/4G)^{1/2} > h_0$, and the results show that the strain to failure peaks at a high cross-linking density and for small graphene sheets (Figure 4c). Specifically, the VCB2 and CB cross-links lead to high strain to failure (~30 and 25%, respectively) at the OCD for the tensile strength due to their high shear strain to failure, γ_{cr} (Figure 4b,c).

Additional Remarks on the Effects of Microstructural Characteristics. With the mechanical properties of graphene-derived LbL materials predicted from our DTS model and results reported in recent experimental studies,[17,55−66] we summarize the current status of material design in Figure 6.
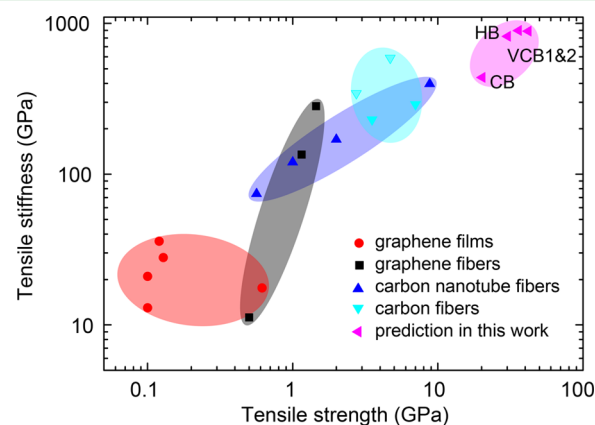

Figure 6. Overall tensile stiffness and strength of graphene-derived LbL materials. The data are collected from the literature for graphene films and fibers, carbon nanotube fibers and the carbon fiber,[17,55−66] and the results obtained in this work.

The survey shows that our theoretical predictions suggest that these materials are highly promising, surpassing the carbon fibers, although the present synthesis and fabrication processes limit their mechanical performance, wherein the ideal model illustrated in Figure 1 cannot be well controlled. In the previous discussion, a regular LbL structure is considered and the effects of wrinkles in the sheets and nonuniform distribution of the surface functional groups have not been taken into account, which, however, are typical microstructural features of graphene-derived materials and are responsible for further weakening of the sheets and/or interfacial load transfer locally

(Figure S5).[17,55] Specifically, the formation of wrinkles break down the load transfer path within the graphene sheets, which can be considered as the reduction of sheet size l in our DTS model and could reduce the overall performance of graphene-derived LbL materials. For example, for the HB-cross-linked sheets with $\phi = 1\%$, the formation of a single wrinkle in the graphene sheet with lateral size $l = 10$ nm results in 60.2% reduction in Y_{eff} and 41.7% reduction in the tensile strength, σ_s. The functional groups on the graphene sheets may form clusters in the basal plane, becoming more adhesive to the neighboring layers but more detrimental to their in-plane mechanical resistance. As a result, the local interlayer load transfer could be enhanced but the intralayer mechanical resistance is reduced, which can be considered as a "renormalized" cross-link with a lower density. With these irregularities considered in our DTS model, we could explain the fact that from experimental reports in the literature, the characteristic lateral size of graphene sheets is ∼1−50 μm,[56] whereas the value is only ∼0.01−1 μm in our theoretical predictions without considering the microstructural features as discussed above.

CONCLUSIONS

To summarize, we explored the overall mechanical properties of graphene-derived LbL materials with interlayer cross-links by three representative functional groups on graphene, on the basis of first-principles calculations and continuum model-based analysis. The irregular microstructural features neglected in the ideal model are also discussed, which explains the relatively low performance reported in the literature and demonstrates the superior performance of the material if its microstructures can be finely controlled in the fabrication processes. Although our discussion is limited in the low-cross-linking-density regime, the conclusions could be extended to high concentrations as well, wherein more cooperative effects such as clustering of functional groups in graphene and interfacial self-healing upon loading may be activated.[1] Moreover, the effects of irregularity in the graphene sheet size and arrangement in determining the mechanical properties of the LbL assemblies could be further probed using the current model, as has been done for biological materials such as bones and carbon nanotube bundles.[19,26,28] The OCDs to maximize the effective tensile stiffness and tensile strength are predicted, and the effects of microstructural features of graphene sheets on the overall mechanical performance of the films are discussed, offering a rational guide for the design and fabrication of high-performance structural materials with functionalized graphene sheets as building blocks.

ASSOCIATED CONTENT

ⓢ Supporting Information

The Supporting Information is available free of charge on the ACS Publications website at DOI: 10.1021/acsami.7b04411.

> Mechanical properties of CB- and HB-cross-linked structures under shear calculated with van der Waals corrections and plain GGA (Figure S1); tensile stress−strain relations for monolayer and bilayer graphene functionalized by one hydroxyl group per 128 carbon atoms, and tensile stress−strain relation for monolayer graphene calculated with supercell sizes of 1.97 nm × 1.71 nm and 3.94 nm × 1.71 nm (Figure S2); loading paths of the VCB1-, VCB2-, HB-, CB-cross-linked structures upon shear loadings (Figure S3); charge density plots for monolayer functionalized graphene at different strain levels (Figure S4); wrinkles formed in graphene oxide films, and nonuniformly distributed, clustered functional groups on graphene (Figure S5) (PDF)

AUTHOR INFORMATION

Corresponding Authors
*E-mail: yilunliu@mail.xjtu.edu.cn (Y.L.).
*E-mail: xuzp@tsinghua.edu.cn (Z.X.).

ORCID
Enlai Gao: 0000-0003-1960-0260
Zhiping Xu: 0000-0002-2833-1966

Notes
The authors declare no competing financial interest.

ACKNOWLEDGMENTS

REFERENCES

(1) Liu, Y. L.; Xu, Z. P. Multimodal and Self-Healable Interfaces Enable Strong and Tough Graphene-Derived Materials. *J. Mech. Phys. Solids* **2014**, *70*, 30−41.

(2) Liu, Y. L.; Xie, B.; Zhang, Z.; Zheng, Q. S.; Xu, Z. P. Mechanical Properties of Graphene Papers. *J. Mech. Phys. Solids* **2012**, *60*, 591−605.

(3) Wei, X.; Meng, Z.; Ruiz, L.; Xia, W.; Lee, C.; Kysar, J. W.; Hone, J. C.; Keten, S.; Espinosa, H. D. Recoverable Slippage Mechanism in Multilayer Graphene Leads to Repeatable Energy Dissipation. *ACS Nano* **2016**, *10*, 1820−1828.

(4) Xia, W.; Ruiz, L.; Pugno, N. M.; Keten, S. Critical Length Scales and Strain Localization Govern the Mechanical Performance of Multi-Layer Graphene Assemblies. *Nanoscale* **2016**, *8*, 6456−6462.

(5) Wei, X.; Naraghi, M.; Espinosa, H. D. Optimal Length Scales Emerging from Shear Load Transfer in Natural Materials: Application to Carbon-Based Nanocomposite Design. *ACS Nano* **2012**, *6*, 2333−2344.

(6) Stankovich, S.; Dikin, D. A.; Dommett, G. H.; Kohlhaas, K. M.; Zimney, E. J.; Stach, E. A.; Piner, R. D.; Nguyen, S. T.; Ruoff, R. S. Graphene-Based Composite Materials. *Nature* **2006**, *442*, 282−286.

(7) Young, R. J.; Kinloch, I. A.; Gong, L.; Novoselov, K. S. The Mechanics of Graphene Nanocomposites: A Review. *Compos. Sci. Technol.* **2012**, *72*, 1459−1476.

(8) Gong, L.; Kinloch, I. A.; Young, R. J.; Riaz, I.; Jalil, R.; Novoselov, K. S. Interfacial Stress Transfer in a Graphene Monolayer Nano-composite. *Adv. Mater.* **2010**, *22*, 2694−2697.

(9) Kotov, N. A.; Dekany, I.; Fendler, J. H. Ultrathin Graphite Oxide-Polyelectrolyte Composites Prepared by Self-Assembly: Transition between Conductive and Non-Conductive States. *Adv. Mater.* **1996**, *8*, 637−641.

(10) Zhao, X.; Xu, Z.; Zheng, B. N.; Gao, C. Macroscopic Assembled, Ultrastrong and H_2SO_4-Resistant Fibres of Polymer-Grafted Graphene Oxide. *Sci. Rep.* **2013**, *3*, No. 3164.

(11) An, Z.; Compton, O. C.; Putz, K. W.; Brinson, L. C.; Nguyen, S. T. Bio-Inspired Borate Cross-Linking in Ultra-Stiff Graphene Oxide Thin Films. *Adv. Mater.* **2011**, *23*, 3842−3846.

(12) Compton, O. C.; Cranford, S. W.; Putz, K. W.; An, Z.; Brinson, L. C.; Buehler, M. J.; Nguyen, S. T. Tuning the Mechanical Properties of Graphene Oxide Paper and Its Associated Polymer Nanocomposites by Controlling Cooperative Intersheet Hydrogen Bonding. *ACS Nano* 2012, 6, 2008–2019.

(13) Qiu, L.; Liu, J. Z.; Chang, S. L.; Wu, Y.; Li, D. Biomimetic Superelastic Graphene-Based Cellular Monoliths. *Nat. Commun.* 2012, 3, No. 1241.

(14) Li, Y. Q.; Yu, T.; Yang, T. Y.; Zheng, L. X.; Liao, K. Bio-Inspired Nacre-Like Composite Films Based on Graphene with Superior Mechanical, Electrical, and Biocompatible Properties. *Adv. Mater.* 2012, 24, 3426–3431.

(15) Lin, X.; Shen, X.; Sun, X.; Liu, X.; Wu, Y.; Wang, Z.; Kim, J. K. Graphene Oxide Papers Simultaneously Doped with Mg(2+) and Cl(-) for Exceptional Mechanical, Electrical, and Dielectric Properties. *ACS Appl. Mater. Interfaces* 2016, 8, 2360–2371.

(16) Xu, Z.; Gao, C. Graphene Chiral Liquid Crystals and Macroscopic Assembled Fibres. *Nat. Commun.* 2011, 2, No. 571.

(17) Xu, Z.; Sun, H.; Zhao, X.; Gao, C. Ultrastrong Fibers Assembled from Giant Graphene Oxide Sheets. *Adv. Mater.* 2013, 25, 188–193.

(18) Gao, H. J. Application of Fracture Mechanics Concepts to Hierarchical Biomechanics of Bone and Bone-Like Materials. *Int. J. Fract.* 2006, 138, 101–137.

(19) Zhang, Z.; Zhang, Y. W.; Gao, H. On Optimal Hierarchy of Load-Bearing Biological Materials. *Proc. Biol. Sci.* 2011, 278, 519–525.

(20) Zuo, S.; Wei, Y. G. Effective Elastic Modulus of Bone-Like Hierarchical Materials. *Acta Mech. Solida Sin.* 2007, 20, 198–205.

(21) Zhong, D.; Yang, Q.; Guo, L.; Dou, S.; Liu, K.; Jiang, L. Fusion of Nacre, Mussel, and Lotus Leaf: Bio-Inspired Graphene Composite Paper with Multifunctional Integration. *Nanoscale* 2013, 5, 5758–5764.

(22) Finnemore, A.; Cunha, P.; Shean, T.; Vignolini, S.; Guldin, S.; Oyen, M.; Steiner, U. Biomimetic Layer-by-Layer Assembly of Artificial Nacre. *Nat. Commun.* 2012, 3, No. 966.

(23) Cheng, Q.; Wu, M.; Li, M.; Jiang, L.; Tang, Z. Ultratough Artificial Nacre Based on Conjugated Cross-Linked Graphene Oxide. *Angew. Chem., Int. Ed. Engl.* 2013, 52, 3750–3755.

(24) Dimas, L. S.; Bratzel, G. H.; Eylon, I.; Buehler, M. J. Tough Composites Inspired by Mineralized Natural Materials: Computation, 3D Printing, and Testing. *Adv. Funct. Mater.* 2013, 23, 4629–4638.

(25) Yao, H. M.; Song, Z. G.; Xu, Z. P.; Gao, H. J. Cracks Fail to Intensify Stress in Nacreous Composites. *Compos. Sci. Technol.* 2013, 81, 24–29.

(26) Zhang, Z. Q.; Liu, B.; Huang, Y.; Hwang, K. C.; Gao, H. Mechanical Properties of Unidirectional Nanocomposites with Non-Uniformly or Randomly Staggered Platelet Distribution. *J. Mech. Phys. Solids* 2010, 58, 1646–1660.

(27) Ji, B. H.; Gao, H. J. Mechanical Properties of Nanostructure of Biological Materials. *J. Mech. Phys. Solids* 2004, 52, 1963–1990.

(28) Zhang, Z. Q.; Liu, B.; Zhang, Y. W.; Hwang, K. C.; Gao, H. J. Ultra-Strong Collagen-Mimic Carbon Nanotube Bundles. *Carbon* 2014, 77, 1040–1053.

(29) Kis, A.; Csanyi, G.; Salvetat, J. P.; Lee, T. N.; Couteau, E.; Kulik, A. J.; Benoit, W.; Brugger, J.; Forro, L. Reinforcement of Single-Walled Carbon Nanotube Bundles by Intertube Bridging. *Nat. Mater.* 2004, 3, 153–157.

(30) Salvetat, J. P.; Briggs, G. A. D.; Bonard, J. M.; Bacsa, R. R.; Kulik, A. J.; Stockli, T.; Burnham, N. A.; Forro, L. Elastic and Shear Moduli of Single-Walled Carbon Nanotube Ropes. *Phys. Rev. Lett.* 1999, 82, 944–947.

(31) Gao, Y.; Liu, L. Q.; Zu, S. Z.; Peng, K.; Zhou, D.; Han, B. H.; Zhang, Z. The Effect of Interlayer Adhesion on the Mechanical Behaviors of Macroscopic Graphene Oxide Papers. *ACS Nano* 2011, 5, 2134–2141.

(32) Park, S.; Lee, K. S.; Bozoklu, G.; Cai, W.; Nguyen, S. T.; Ruoff, R. S. Graphene Oxide Papers Modified by Divalent Ions-Enhancing Mechanical Properties via Chemical Cross-Linking. *ACS Nano* 2008, 2, 572–578.

(33) Liu, Y. L.; Xie, B.; Xu, Z. P. Mechanics of Coordinative Crosslinks in Graphene Nanocomposites: A First-Principles Study. *J. Mater. Chem.* 2011, 21, 6707–6712.

(34) Liu, L.; Gao, Y.; Liu, Q.; Kuang, J.; Zhou, D.; Ju, S.; Han, B.; Zhang, Z. High Mechanical Performance of Layered Graphene Oxide/Poly(Vinyl Alcohol) Nanocomposite Films. *Small* 2013, 9, 2466–2472.

(35) Bekyarova, E.; Sarkar, S.; Wang, F.; Itkis, M. E.; Kalinina, I.; Tian, X.; Haddon, R. C. Effect of Covalent Chemistry on the Electronic Structure and Properties of Carbon Nanotubes and Graphene. *Acc. Chem. Res.* 2013, 46, 65–76.

(36) Mark, J. E.; Erman, B. *Rubberlike Elasticity: A Molecular Primer*; Cambridge University Press: Cambridge, 2007.

(37) Hartmann, M. A.; Fratzl, P. Sacrificial Ionic Bonds Need to Be Randomly Distributed to Provide Shear Deformability. *Nano Lett.* 2009, 9, 3603–3607.

(38) Wojtecki, R. J.; Meador, M. A.; Rowan, S. J. Using the Dynamic Bond to Access Macroscopically Responsive Structurally Dynamic Polymers. *Nat. Mater.* 2011, 10, 14–27.

(39) Medhekar, N. V.; Ramasubramaniam, A.; Ruoff, R. S.; Shenoy, V. B. Hydrogen Bond Networks in Graphene Oxide Composite Paper: Structure and Mechanical Properties. *ACS Nano* 2010, 4, 2300–2306.

(40) Wang, C.; Wang, L. F.; Xu, Z. P. Enhanced Mechanical Properties of Carbon Nanotube Networks by Mobile and Discrete Binders. *Carbon* 2013, 64, 237–244.

(41) Dimiev, A. M.; Tour, J. M. Mechanism of Graphene Oxide Formation. *ACS Nano* 2014, 8, 3060–3068.

(42) Faucett, A. C.; Mativetsky, J. M. Nanoscale Reduction of Graphene Oxide under Ambient Conditions. *Carbon* 2015, 95, 1069–1075.

(43) Trevethan, T.; Dyulgerova, P.; Latham, C. D.; Heggie, M. I.; Seabourne, C. R.; Scott, A. J.; Briddon, P. R.; Rayson, M. J. Extended Interplanar Linking in Graphite Formed from Vacancy Aggregates. *Phys. Rev. Lett.* 2013, 111, No. 095501.

(44) Jin, E. Z.; He, J. Y.; Sheng, K. X.; Zhang, Z. L.; Shi, G. Q.; Zheng, Q. S. Electron-Irradiation-Induced Reinforcement of Reduced Graphene Oxide Papers. *Acta Mater.* 2013, 61, 6466–6473.

(45) Gao, W.; Alemany, L. B.; Ci, L.; Ajayan, P. M. New Insights into the Structure and Reduction of Graphite Oxide. *Nat. Chem.* 2009, 1, 403–408.

(46) Perdew, J. P.; Burke, K.; Ernzerhof, M. Generalized Gradient Approximation Made Simple. *Phys. Rev. Lett.* 1996, 77, 3865–3868.

(47) Grimme, S.; Antony, J.; Ehrlich, S.; Krieg, H. A Consistent and Accurate Ab Initio Parametrization of Density Functional Dispersion Correction (DFT-D) for the 94 Elements H-Pu. *J. Chem. Phys.* 2010, 132, No. 154104.

(48) Grimme, S.; Ehrlich, S.; Goerigk, L. Effect of the Damping Function in Dispersion Corrected Density Functional Theory. *J. Comput. Chem.* 2011, 32, 1456–1465.

(49) Blöchl, P. E. Projector Augmented-Wave Method. *Phys. Rev. B: Condens. Matter Mater. Phys.* 1994, 50, 17953–17979.

(50) Kresse, G.; Furthmüller, J. Efficient Iterative Schemes Forab Initiototal-Energy Calculations Using a Plane-Wave Basis Set. *Phys. Rev. B: Condens. Matter Mater. Phys.* 1996, 54, 11169–11186.

(51) Xu, Z. Mechanics of Metal-Catecholate Complexes: The Roles of Coordination State and Metal Types. *Sci. Rep.* 2013, 3, No. 2914.

(52) Song, Z. G.; Xu, Z. P. Geometrical Effect 'Stiffens' Graphene Membrane at Finite Vacancy Concentrations. *Extreme Mech. Lett.* 2016, 6, 82–87.

(53) Wang, M. C.; Yan, C.; Ma, L.; Hu, N.; Chen, M. W. Effect of Defects on Fracture Strength of Graphene Sheets. *Comput. Mater. Sci.* 2012, 54, 236–239.

(54) Dewapriya, M. A. N.; Rajapakse, R. K. N. D. Molecular Dynamics Simulations and Continuum Modeling of Temperature and Strain Rate Dependent Fracture Strength of Graphene with Vacancy Defects. *J. Appl. Mech.* 2014, 81, No. 081010.

(55) Zhang, M.; Wang, Y.; Huang, L.; Xu, Z.; Li, C.; Shi, G. Multifunctional Pristine Chemically Modified Graphene Films as Strong as Stainless Steel. *Adv. Mater.* 2015, 27, 6708–6713.

(56) Lin, X.; Shen, X.; Zheng, Q.; Yousefi, N.; Ye, L.; Mai, Y. W.; Kim, J. K. Fabrication of Highly-Aligned, Conductive, and Strong Graphene Papers Using Ultralarge Graphene Oxide Sheets. *ACS Nano* **2012**, *6*, 10708−10719.

(57) Xu, Z.; Liu, Y.; Zhao, X.; Peng, L.; Sun, H.; Xu, Y.; Ren, X.; Jin, C.; Xu, P.; Wang, M.; Gao, C. Ultrastiff and Strong Graphene Fibers Via Full-Scale Synergetic Defect Engineering. *Adv. Mater.* **2016**, *28*, 6449−6456.

(58) Di, J.; Fang, S.; Moura, F. A.; Galvao, D. S.; Bykova, J.; Aliev, A.; de Andrade, M. J.; Lepro, X.; Li, N.; Haines, C.; Ovalle-Robles, R.; Qian, D.; Baughman, R. H. Strong, Twist-Stable Carbon Nanotube Yarns and Muscles by Tension Annealing at Extreme Temperatures. *Adv. Mater.* **2016**, *28*, 6598−6605.

(59) Xin, G.; Yao, T.; Sun, H.; Scott, S. M.; Shao, D.; Wang, G.; Lian, J. Highly Thermally Conductive and Mechanically Strong Graphene Fibers. *Science* **2015**, *349*, 1083−1087.

(60) Cheng, Q.; Jiang, L.; Tang, Z. Bioinspired Layered Materials with Superior Mechanical Performance. *Acc. Chem. Res.* **2014**, *47*, 1256−1266.

(61) Behabtu, N.; Young, C. C.; Tsentalovich, D. E.; Kleinerman, O.; Wang, X.; Ma, A. W.; Bengio, E. A.; ter Waarbeek, R. F.; de Jong, J. J.; Hoogerwerf, R. E.; Fairchild, S. B.; Ferguson, J. B.; Maruyama, B.; Kono, J.; Talmon, Y.; Cohen, Y.; Otto, M. J.; Pasquali, M. Strong, Light, Multifunctional Fibers of Carbon Nanotubes with Ultrahigh Conductivity. *Science* **2013**, *339*, 182−186.

(62) Lu, W.; Zu, M.; Byun, J. H.; Kim, B. S.; Chou, T. W. State of the Art of Carbon Nanotube Fibers: Opportunities and Challenges. *Adv. Mater.* **2012**, *24*, 1805−1833.

(63) He, F. *Carbon Fiber and Graphite Fiber* (in Chinese); Chemical Industry Press: Beijing, 2010.

(64) Dikin, D. A.; Stankovich, S.; Zimney, E. J.; Piner, R. D.; Dommett, G. H.; Evmenenko, G.; Nguyen, S. T.; Ruoff, R. S. Preparation and Characterization of Graphene Oxide Paper. *Nature* **2007**, *448*, 457−460.

(65) Zhang, X. B.; Jiang, K. L.; Teng, C.; Liu, P.; Zhang, L.; Kong, J.; Zhang, T. H.; Li, Q. Q.; Fan, S. S. Spinning and Processing Continuous Yarns from 4-Inch Wafer Scale Super-Aligned Carbon Nanotube Arrays. *Adv. Mater.* **2006**, *18*, 1505−1510.

(66) Dai, Z. H.; Wang, Y. L.; Liu, L. Q.; Liu, X. L.; Tan, P. H.; Xu, Z. P.; Kuang, J.; Liu, Q.; Lou, J.; Zhang, Z. Hierarchical Graphene-Based Films with Dynamic Self-Stiffening for Biomimetic Artificial Muscle. *Adv. Funct. Mater.* **2016**, *26*, 7003−7010.

Supporting Information

Optimizing Interfacial Crosslinking in Graphene-derived Materials that Balances Intralayer and Interlayer Load Transfer

Enlai Gao[1], Yu Cao[2], Yilun Liu[3,*], and Zhiping Xu[1,*]

[1]Applied Mechanics Laboratory, Department of Engineering Mechanics and Center for Nano and Micro Mechanics, Tsinghua University, Beijing 100084, China.

[2]College of Chemistry, Nankai University, Tianjin 300071, China.

[3]State Key Laboratory for Strength and Vibration of Mechanical Structures, School of Aerospace Engineering, Xi'an Jiaotong University, Xi'an 710049, China.

[*]Corresponding authors. Email: xuzp@tsinghua.edu.cn, yilunliu@mail.xjtu.edu.cn

This Supplementary Information Material contains
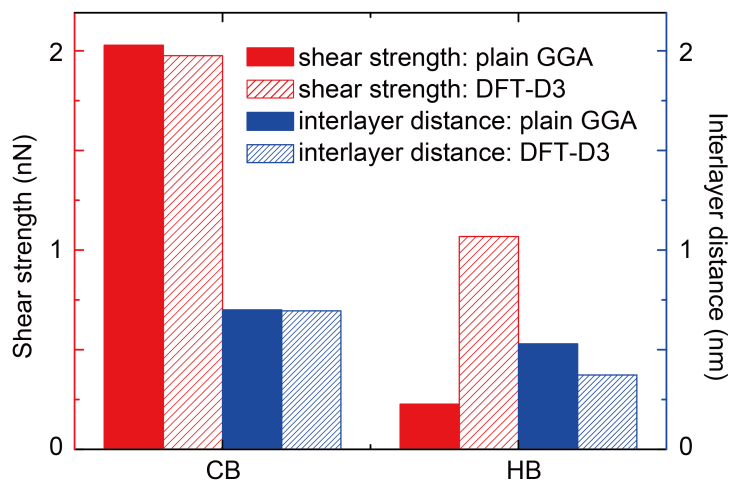
- Supplementary Figures S1-S5.

Figure S1. The shear strength and interlayer distance calculated for CB- and HB-crosslinked structures, with van der Waals corrections using the DFT-D3 method, compared to the results obtained with plain GGA.
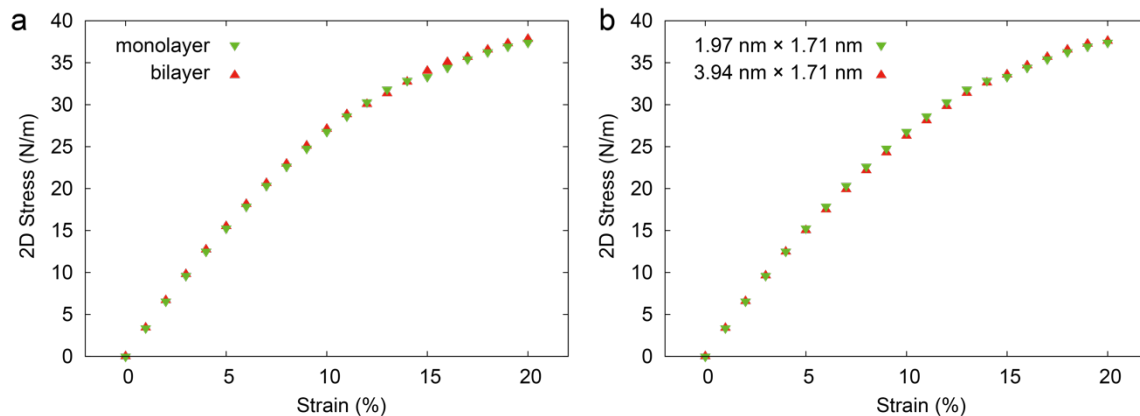
Figure S2. (a) Two-dimensional (2D) tensile stress-strain relation for monolayer and bilayer graphene functionalized by one hydroxyl group per 128 carbon atoms, forming a HB crosslink in the bilayer composite. (b) 2D tensile stress-strain relation for monolayer graphene calculated with supercell sizes of 1.97 nm × 1.71 nm and 3.94 nm × 1.71nm.
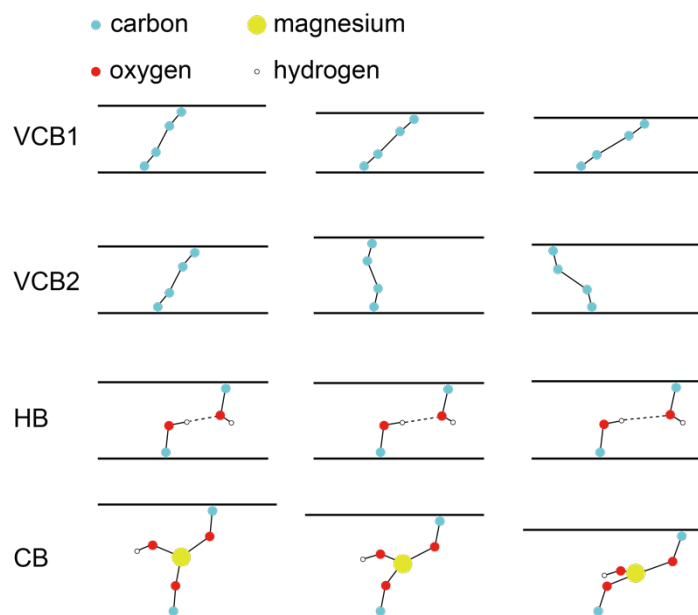
Figure S3. Structural distortion of the VCB1-, VCB2-, HB-, CB-crosslinked structures upon shear loading (in different directions, the upper graphene layer is displaced rightward and leftward for VCB1 and VCB2, respectively).
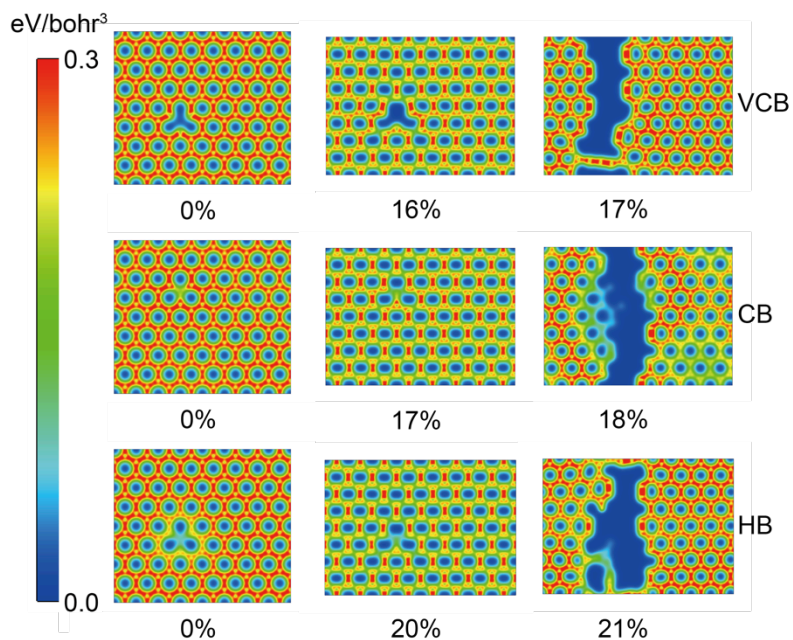
Figure S4. Charge density plots for monolayer graphene (in the basal plane) functionalized by VCB-, CB- and HB-crosslinks at different strain levels, which demonstrates the charge depletion during crack nucleation and propagation processes.
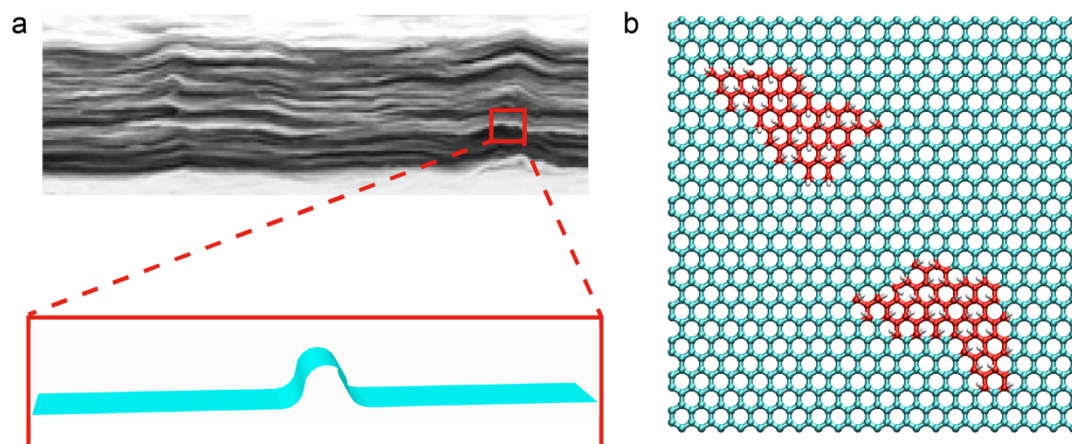
Figure S5. (a) Wrinkles formed in graphene oxide films, shown in the scanning electron microscopy (SEM) image and model illustration. (b) Non-uniformly distributed, clustered functional groups on graphene.